IEEE Access
Multidisciplinary | Rapid Review | Open Access Journal

Received August 8, 2019, accepted August 28, 2019, date of publication September 11, 2019, date of current version September 23, 2019.

Digital Object Identifier 10.1109/ACCESS.2019.2940381

Perceptual Vibration Hashing by Sub-Band Coding: An Edge Computing Method for Condition Monitoring

HAINING LIU[1,2], YIXIANG WANG[1], FAJIA LI[1], XIAOHONG WANG[3], CHENGLIANG LIU[4], AND MICHAEL G. PECHT[2], (Fellow, IEEE)

[1]School of Mechanical Engineering, University of Jinan, Jinan 250022, China
[2]Center for Advanced Life Cycle Engineering, University of Maryland at College Park, College Park, MD 20742, USA
[3]School of Electrical Engineering, University of Jinan, Jinan 250022, China
[4]School of Mechanical Engineering, Shanghai Jiao Tong University, Shanghai 200240, China

Corresponding author: Haining Liu (ujnlhn@gmail.com)

This work was supported in part by the National Natural Science Foundation of China under Grant 51605191, in part by the Shandong Provincial Key Research and Development Program under Grant 2019GGX105009, in part by the Shandong Provincial Natural Science Foundation under Grant ZR2016EEB37, and in part by the China Scholarship Council under Grant 201808370045.

ABSTRACT High data throughput during real-time vibration monitoring can easily lead to network congestion, insufficient data storage space, heavy computing burden, and high communication costs. As a new computing paradigm, edge computing is deemed to be a good solution to these problems. In this paper, perceptual hashing is proposed as an edge computing form, aiming not only to reduce the data dimensionality but also to extract and represent the machine condition information. A sub-band coding method based on wavelet packet transform, two-dimensional discrete cosine transform, and symbolic aggregate approximation is developed for perceptual vibration hashing. When the sub-band coding method is implemented on a monitoring terminal, the acquired kilobyte-long vibration signal can be transformed into a machine condition hash occupying only a few bytes. Therefore, the efficiency of condition monitoring can benefit from the compactness of the machine condition hash, while comparable diagnostic and prognostic results can still be achieved. The effectiveness of the developed method is verified with two benchmark bearing datasets. Considerations on practical condition monitoring applications are also presented.

INDEX TERMS Prognostics and health management (PHM), condition monitoring, edge computing, bearing fault diagnosis, degradation assessment, perceptual hashing, wavelet packet transform, discrete cosine transform, symbolic aggregate approximation (SAX).

I. INTRODUCTION

Condition monitoring is a systematic project which includes a series of processes: data acquisition, transmission, storage, processing, condition recognition, and visualization. Although different solutions have been developed [1]–[3], a terminal-server-client architecture is commonly followed for network-based condition monitoring. The terminal, which is generally embedded in a machine along with various sensors, is used for data acquisition and transmission; the remote server is set up for data receiving, storage, processing, and condition recognition; and the client can be a PC or a mobile device with a human-machine interface (HMI) for visualization of the monitored data and the condition recognition results. During a condition monitoring process, the monitored data flows continuously and automatically, and thus the machine condition information needs to be revealed and recognized in real-time.

However, some technical predicaments may be encountered when putting this architecture into practice, especially for condition monitoring with parameters sampled under high frequency, such as vibration. The network can become congested, especially in concurrent monitoring scenarios, such as a cluster of pumps, or hundreds of wind turbines in a farm. Storage space may be insufficient because data volume grows exponentially with time and the number of monitoring objects. The computing burden is heavy, and the time delay would thus be longer if centralized computing is adopted

The associate editor coordinating the review of this manuscript and approving it for publication was Gongbo Zhou.

to run a diagnostic model. Finally, communication costs are higher when a mobile communication solution is used for data transmission in monitoring mobile objects (e.g., high-speed trains, engineering machinery), or objects for which wired network deployment is difficult (e.g., wind turbines, offshore platforms).

Edge computing [4], [5] aims to solve the above technical predicaments by offloading some preliminary computing tasks to the edge of the network. However, edge computing is somewhat abstract, so the question is what practical edge computing method should be developed for condition monitoring? In order to solve the problem of low efficiency caused by high-frequency sampling, the dimensionality of the acquired data needs to be reduced as much as possible, meanwhile the machine condition information should be extracted as much as possible. Theoretically, the information density of the transmitted data should be improved by edge computing.

In the data-driven fault diagnostics and prognostics, a feature is a compact representation of the machine condition information, with which empirical knowledge or a statistical model can be built for machine condition recognition. Various features have been proposed based on the physics of failure. Statistical parameters in the time and frequency domain are straightforward for vibration monitoring, such as root mean square (RMS), kurtosis, skewness, and crest factor. Time-frequency joint analysis methods are widely studied and employed because they are able to uncover the latent diagnostic information in nonstationary signals. The most common ones include short-time Fourier transform (STFT), wavelet-based methods [6], [7], and empirical mode decomposition (EMD) [8]. Advanced features are also proposed, such as spectral kurtosis [9] and Rényi entropy [10]. However, one feature represents one aspect of a system's dynamic behavior. In order to represent machine condition information comprehensively, multiple features are extracted, and then feature selection or dimensionality reduction proceeds. For instance, Malhi and Gao [11] devised a systematic feature selection scheme based on principal component analysis (PCA) to fuse features from time, frequency, and wavelet domains for bearing condition monitoring; Rauber *et al.* [12] developed a feature selection method by searching the heterogeneous feature space with diagnostic performance criteria. A review of feature selection methods can be found in [13]. Feature extraction and selection is substantially a process to reveal the machine condition information.

Can edge computing at the terminal, therefore, be instantiated as one of the feature extraction and selection methods above? The answer may be yes, but the efficiency and effectiveness of condition monitoring may still be constrained. First of all, monitoring terminals are usually limited in computing resources, multi-feature extraction and selection may increase the latency in real-time monitoring, and advanced methods may be inapplicable. Furthermore, a fixed diagnostic/prognostic model cannot adapt to complex working conditions and the diversity of failure modes, i.e., the feature extraction or information revealing method may need to be updated to meet the classification or regression requirements. Last but not least, the choice of the feature extraction and selection method on a terminal depends on how the machine condition information is used for condition recognition on a monitoring server. That is, the coupling of feature engineering and condition recognition in data-driven fault diagnostic or prognostic modeling can limit the technical implementation of condition monitoring. Eventually, to achieve reasonable diagnostic/prognostic modeling, the application of edge computing for condition monitoring should be systematically considered.

In summary, although edge computing provides a conceptual paradigm to improve the efficiency of condition monitoring, its successful implementation should comprehensively consider its effectiveness in machine condition information extraction, dimension reduction, computing efficiency, and flexibility in machine condition inference. Following the methodology of perceptual hashing, a sub-band coding method was developed in this paper as an edge computing instance. Vibration signal is mainly focused on because it is commonly used for machine condition monitoring. The main contributions of this paper include: perceptual hashing is formally introduced as an edge computing form for machine condition information extraction and representation, which leads to a new framework for diagnosis and prognosis; a sub-band coding method is developed for perceptual vibration hashing, in which although conventional wavelet packet transform (WPT) and two-dimensional discrete cosine transform (2D-DCT) are adopted for sub-band division and feature extraction, the aggregate approximation (SAX) can compactly represent the sub-band feature in a symbolic way, then condition monitoring efficiency can be improved; a new form of machine condition hash is defined as the information carrier exchanged between the monitoring terminal and the server, with which the condition inference on the server can be decoupled from the machine condition hash generation on the terminal.

The rest of the paper is organized as follows. In Section II, the framework for diagnosis and prognosis based on perceptual hashing is briefly reviewed. Theoretical foundations about sub-band coding, wavelet packet transform, two-dimensional discrete cosine transform, and symbolic aggregate approximation are introduced in Section III. The developed perceptual vibration hashing method based on sub-band coding is introduced in Section IV, and then verified in Section V by applying it for bearing fault diagnosis and degradation assessment. Discussion and conclusions are presented in Sections VI.

II. DIAGNOSIS AND PROGNOSIS BASED ON PERCEPTUAL HASHING

Generally, a hash function encodes data of arbitrary size into a small, fixed-size representation. For some hashing algorithms, such as MD5, SHA-1, and SHA256, a small change in the input data would perturb the hashing result completely, which makes them adequate for applications such

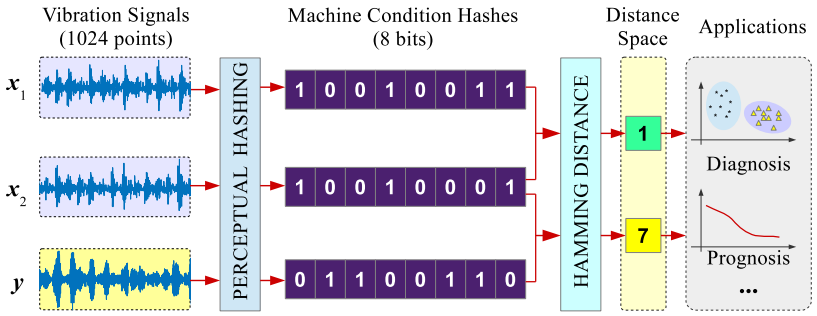

FIGURE 1. A new famework for diagnosis and prognosis based on perceptual hashing.

as cryptography, information retrieval, and file verification. However, perceptual hashing is different because it hashes the meaningful information in the data rather than the raw data itself and even makes the hashed information comparable by defining distance functions on the hash codes. Although different terms are used in the literature, such as "binary hashing" [14] or "hashing" [15], "perceptual hashing" [16] is preferred here because it implies an information-oriented way of hashing.

Three computing characteristics make perceptual hashing an optimal choice for condition monitoring: compactness, robustness, and discriminability. Compactness exists in the hash codes, which means a low-dimensional representation, or a "short hash code," is used to represent the extracted information or content so that it can be easily transmitted, stored, and computed. With regard to robustness and discriminability, a distance function needs to be defined as the criterion. When processing data with similar information or content, the generated hash codes should be close, or "robust," in the defined distance space, even though they may appear differently in representations. However, when processing different information or content, the distance will increase so that the data can be discriminated.

Taking the vibration monitoring of bearings as an example, for vibration signals $\boldsymbol{x}_1$ and $\boldsymbol{x}_2$ sampled under the same bearing condition in Fig. 1, similar machine condition hashes should be generated. In this example, the similarity is quantized by the bitwise Hamming distance. However, the distance will increase when the bearing deviates from its original condition. Fig. 1 shows that the Hamming distance is 7 between $\boldsymbol{x}_2$ and $\boldsymbol{y}$, which is greater than the distance between $\boldsymbol{x}_1$ and $\boldsymbol{x}_2$ because $\boldsymbol{y}$ is sampled from a different bearing condition. Fault diagnosis and prognosis can therefore be performed in the distance space of machine condition hashes, which leads to a new diagnostic and prognostic framework.

The hypothesis behind applying perceptual hashing as an edge computing method for condition monitoring is that the machine condition would mostly be maintained at a relatively healthy status, so the generated machine condition hashes would be close in their distance space. However, when the machine condition degrades into one failure mode, the generated machine condition hashes would gradually deviate from its healthy position in the distance space, but meanwhile far from other faulty types so that fault classification can be achieved. Computing efficiency is also desired because the monitoring terminals are usually limited in computing resources. Technically, perceptual hashing can be implemented on a monitoring terminal, while diagnosis and prognosis can be performed on a server with better computing power. A new condition monitoring architecture was developed by Liu *et al.* [17], in which the machine condition hash was exchanged between the terminal and server to achieve more efficient and flexible condition monitoring.

III. THEORETICAL FOUNDATIONS

In this section, the signal processing techniques used in developing the perceptual vibration hashing are introduced. The sub-band coding is a signal processing scheme commonly used for digital coding, which is followed in this paper for machine condition information extraction and representation. Specifically, wavelet packet transform (WPT), two-dimensional discrete cosine transform (2D-DCT), and symbolic aggregate approximation (SAX) are the sub-band coding methods jointly used for perceptual vibration hashing.

A. SUB-BAND CODING

Sub-band coding (SBC) was originally proposed in [17] and [19] based on the rationale that digital coding in terms of sub-bands in the total spectrum is an improvement over full-band coding. When the channels of a filter bank (i.e., a number of frequency bands) are used for coding, the resulting scheme is known as sub-band coding [20].

Sub-band coding was used to exploit auditory masking of the auditory system. It is an essential procedure for some psychoacoustic models and audio compression schemes. A series of successful audio codes has been developed by dividing a signal into frequency bands that essentially imitate the human auditory system [20]. One example is the MUSICAM (masking pattern adapted universal sub-band integrated coding and multiplexing) system [21], [22], which dynamically quantizes the sub-band samples by discarding all components that cannot be perceived by the human ear.

Nevertheless, the goal of applying sub-band coding for condition monitoring applications is to extract and represent

the machine condition information, rather than the data compression and recovery. The same rationale of sub-band coding is followed in this paper to extract, quantize, and represent the machine condition information, whereas the perceptual criteria are not determined by the human sensory organs but the three computing characteristics listed in Section II–compactness, robustness, and discriminability. Fast algorithms for sub-band coding are also mostly available when orthogonality exists between the basis functions used for signal decomposition.

B. WAVELET PACKET TRANSFORM

From a general perspective of signal processing, wavelet is virtually a bandpass filter that has a constant relative bandwidth or "constant-Q" [23]. However, wavelet transform has a rather poor resolution in the high-frequency region, whereas wavelet packet transform (WPT) enhances the idea of multiresolution analysis and decomposes signals into frequency bands with an arbitrary tree-structured filter bank.

In the WPT, a signal is processed through a cascaded filter bank of high-pass filters $h(n)$, low-pass filters $g(n)$ and downsampling operations. For a WP decomposition with a tree depth of j, 2^j final leaf nodes will be obtained, each corresponding to $(1/2^j)$th of the original bandwidth. An example is shown in Fig. 2, in which a 2-level WP decomposition results in 4 sub-bands. A rigorous mathematical introduction and derivation of WPT can be found in [24].

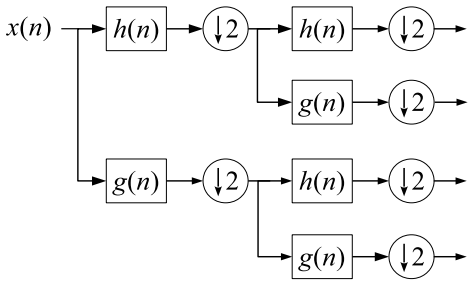

FIGURE 2. Wavelet packet decomposition over 2 levels.

For a finite signal with a length of N, the maximum depth of WP decomposition is $log_2 N$, so it will take $Nlog_2 N$ coefficients of operations at most for a full WP tree. Hence, WPT is chosen as a sub-band division method with the computational efficiency can be guaranteed.

C. 2D DISCRETE COSINE TRANSFORM

Redundancy exists when unnecessary data or wasted spaces are used to represent and transmit certain information. A natural choice to reduce redundancy is to do decorrelation on coefficients in a transformed domain. Theoretically, Karhunen-Loève transform (KLT) can pack most energy into the first k coefficients among all unitary transform, while minimizing the expected distortion [20]. However, its signal dependency and computational complexity make it usually inapplicable in practical applications. The discrete cosine transform (DCT) was developed as the most successful approximation to the KLT in decorrelating signals with Markov-1 statistics [25]. The DCT is therefore adopted in several standards for speech, image, and video compression, such as the Joint Photographic Experts Group (JPEG) and Moving Picture Experts Group (MPEG-2).

First developed by Ahmed *et al.* [26], the DCT has different variants. When coefficient decorrelation is mostly concerned, two-dimensional discrete cosine transform (2D-DCT) is mostly used, which is defined as:

$$X_{uv} = \frac{2c(u)c(v)}{\sqrt{(MN)}} \sum_{m=0}^{M-1} \sum_{n=0}^{N-1} \left(x_{mn} \cos \left[\frac{(2m+1)u\pi}{2M} \right] \times \cos \left[\frac{(2n+1)v\pi}{2N} \right] \right), \quad (1)$$

where $[x]$ is a $M \times N$ matrix, of which the DCT is $[X]$, $u = 0, \cdots, M-1$, $v = 0, \cdots, N-1$, and

$$c(k) = \begin{cases} \frac{1}{\sqrt{2}} & \text{for } k = 0, \\ 1 & \text{otherwise.} \end{cases} \quad (2)$$

Since coefficients of DCT are virtually the real-even data of discrete Fourier transform, most fast algorithms are based on fast Fourier transform (FFT). The computing operation can be reduced to $\frac{17}{9} N \log_2 N + O(N)$ based on a real-data FFT [27].

D. SYMBOLIC AGGREGATE APPROXIMATION

Symbolic aggregate approximation (SAX) is a symbolic representation for time series developed by Lin *et al.* citeLin2003 in 2002. SAX allows for dimensionality reduction and indexing with a lower-bounding distance measure. The main idea of SAX is illustrated with the examples in Fig. 3.

For an n-dimensional time series $\boldsymbol{x} = \{x_1, x_2, \cdots, x_n\}$ ($n = 128$ in Fig. 3a), SAX reduces its dimensionality and represents it with an m-dimensional symbolic sequence $\hat{\boldsymbol{x}} = \{\hat{x}_1, \hat{x}_2, \cdots, \hat{x}_m\}$ by the following sequential procedures:

1) Normalization: The time series $\boldsymbol{x}$ is normalized to $\boldsymbol{x}'$, which has a mean of zero and a standard deviation of one.
2) Dimension reduction via piecewise aggregate approximation (PAA) [29]: In order to reduce the dimensionality of a time series, PAA tries to represent the original time series with the mean values of m equal-sized frames, so that an m-dimensional vector $\bar{\boldsymbol{x}} = \{\bar{x}_1, \bar{x}_2, \cdots, \bar{x}_m\}$ would be obtained, in which $\bar{x}_i$ is calculated as follows:
$$\bar{x}_i = \frac{m}{n} \sum_{j=n/m(i-1)+1}^{(n/m)i} x'_j. \quad (3)$$
3) Discretization: A principle of equiprobability [30], [31] is followed for discretization. Gaussian distribution is assumed in the values of the normalized time series, which is applicable for most families of time series. Then the distribution space under the Gaussian curve

can be divided into k equal-sized areas by $k-1$ breakpoints.

4) Symbolic representation: An alphabet of size k is used to represent the equiprobable regions so that any PAA coefficient that falls into one particular region can be represented with a distinct alpha. Then the PAA vectors $\bar{\boldsymbol{x}}$ would be mapped into a "word" $\hat{\boldsymbol{x}} = \{\hat{x}_1, \hat{x}_2, \cdots, \hat{x}_m\}$, in which:

$$\hat{x}_i = alpha_j, \quad \text{iff.} \quad \beta_{j-1} \le \bar{x}_i < \beta_j, \tag{4}$$

where β_{j-1} and β_j are two adjacent breakpoints.

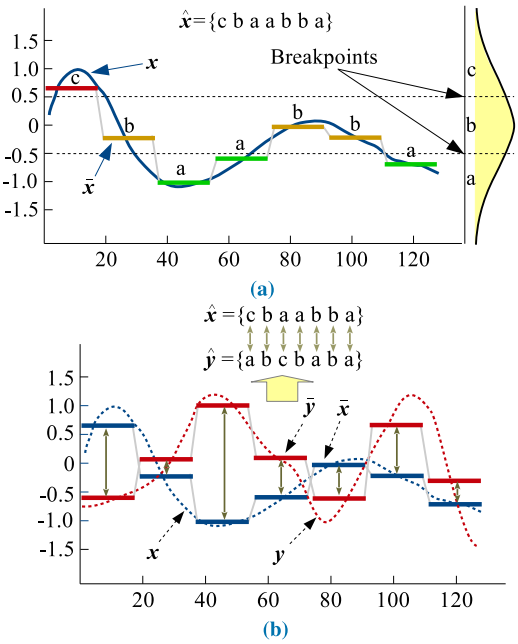

FIGURE 3. An illustration of symbolic aggregate approximation (SAX). (a) The main procedures of SAX: time series (x), piecewise aggregate approximation (PAA) ($\bar{x}$), and symbolic representation ($\hat{x}$). (b) Distance calculation of $\hat{x}$ and $\hat{y}$.

For example, as shown in Fig. 3a, the time series $\boldsymbol{x}$ is first transformed into PAA coefficients $\bar{\boldsymbol{x}}$, with which the dimensionality is reduced. By dividing the Gaussian curve into 3 equiprobable regions with 2 breakpoints, the PAA coefficients $\bar{\boldsymbol{x}}$ are further represented with a 3-length alphabet, i.e., $\hat{\boldsymbol{x}} = \{\text{cbaabba}\}$.

The other privilege of SAX is that a low-bounding [32] distance functions can be defined to quantize the similarity of time series. Given two SAX words $\hat{\boldsymbol{x}}$ and $\hat{\boldsymbol{y}}$ of time series $\boldsymbol{x}$ and $\boldsymbol{y}$ as shown in Fig. 3b, their lower bounding approximation to the Euclidean distance can be defined by accumulating the piecewise distances:

$$\text{MINDIST}(\hat{\boldsymbol{x}}, \hat{\boldsymbol{y}}) \equiv \sqrt{\frac{n}{m}} \sqrt{\sum_{i=1}^{m} \left(\text{dist}\left(\hat{x}_i, \hat{y}_i\right)\right)^2}, \tag{5}$$

in which the $dist()$ function can be implemented using a look-up table as illustrated in Table 1.

TABLE 1. A look-up table for *dist*() function used by MINDIST in (5).

	a	b	c	d
a	0	0	0.67	1.34
b	0	0	0	0.67
c	0.67	0	0	0
d	1.34	0.67	0	0

IV. PERCEPTUAL VIBRATION HASHING WITH SUB-BAND CODING

From filter banks [20] to sparse coding [33], [34], the development of signal processing has continued to draw inspiration from sensory systems about how the human brain efficiently processes nearly gigabit images or audio data with minimized neural resources. In view of the hierarchical organization of cortical sensory systems [35] and the underlying efficient principle in information processing, an integrated perceptual vibration hashing model is developed for condition monitoring (Fig. 4).

Layered machine condition information extraction and representation procedures can be implemented locally after vibration signals are acquired. These procedures include:

1) Sub-band division by WPT: With a j-level WP decomposition and reconstruction, a vibration signal $\boldsymbol{s}$ is divided into 2^j frequency bands. As shown in Fig. 4, a collection of sub-band signals $\boldsymbol{s}_1, \boldsymbol{s}_2, \cdots, \boldsymbol{s}_{2^j}$ is obtained in the divided frequency bands.
2) Blocking: A specific sub-band signal $\boldsymbol{s}_i$, which has a certain frequency range, is truncated into several blocks to make a sub-band matrix for 2D-DCT. For example, in Fig. 4, the reconstructed sub-band signal $\boldsymbol{s}_3$ is truncated into 4 blocks to make a sub-band matrix $\tilde{\boldsymbol{s}}_3 = [\boldsymbol{s}_3^1; \boldsymbol{s}_3^2; \boldsymbol{s}_3^3; \boldsymbol{s}_3^4]$.
3) 2D-DCT: In each frequency band, a stable coefficient matrix $\boldsymbol{f}_i = [\boldsymbol{f}_i^1; \boldsymbol{f}_i^2; \boldsymbol{f}_i^3; \boldsymbol{f}_i^4]$ would be obtained with 2D-DCT by taking advantage of its capability in coefficient decorrelation and energy compaction.
4) Feature extraction: Extract a feature vector $\boldsymbol{a}_i = [a_i^1, a_i^2, \cdots, a_i^p]$ from the ith sub-band coefficients $\boldsymbol{f}_i$, and cascade them together as a sub-band feature vector $\boldsymbol{a} = [\boldsymbol{a}_1, \boldsymbol{a}_2, \cdots, \boldsymbol{a}_{2^j}]$ for the original signal $\boldsymbol{s}$.
5) Hashing with SAX: The machine condition hash, i.e., a symbolic representation of $\boldsymbol{a}$, is obtained by SAX, so that the dimensionality could be further reduced while the main information is preserved but easier to transmit.

Eventually, a piece of the vibration signal with 1024 data points can be transformed into a compact machine condition hash with few characters. For example, if $j = 5$ for wavelet packet decomposition and $p = 4$ for feature extraction in each sub-band, a 128-dimensional sub-band feature vector could be obtained, and then a 32-dimensional machine condition hash would be generated if $m = 32$ for PAA. For an embedded condition monitoring terminal, which may use 4 bytes to store a float-type data point, it will take $1024 \times 4 = 4096$ bytes to store one piece of vibration signal, but only

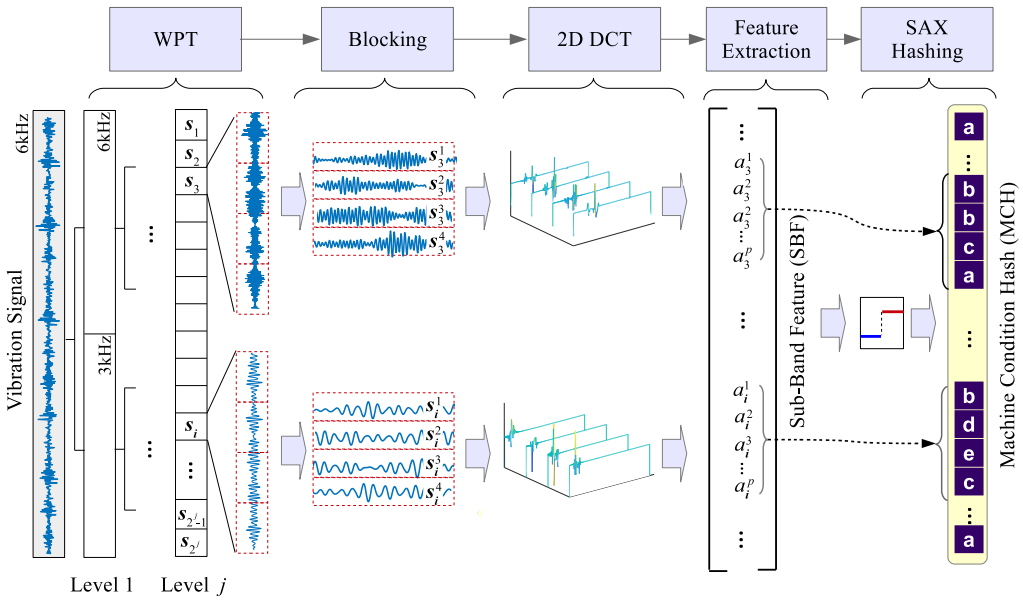

FIGURE 4. Flowchart of sub-band coding for perceptual vibration hashing.

32 bytes of ASCII characters (i.e., machine condition hash) are needed to represent the machine condition information. Fault diagnosis and prognosis can still be performed in the distance space constructed by machine condition hashes, as presented in Section V.

V. CASE STUDIES

As explained in Section II, three computing characteristics are required for perceptual hashing - compactness, robustness, and discriminability. When applying the developed perceptual vibration hashing method for condition monitoring, its effectiveness in fault diagnosis and prognosis is the most concern. As the compactness of the machine condition hash is self-explanatory, in this section, the robustness and discriminability of the developed perceptual vibration hashing method are verified by applying it for bearing fault diagnosis and degradation assessment. Two benchmark bearing datasets were used: the bearing data set from Case Western Reserve University (CWRU) [36] was used for static fault diagnosis, while the other bearing data set was used for dynamic degradation assessment, which was published by the National Science Foundation Industry/University Cooperative Research Center (NSF I/UCRC) [37].

A. CASE STUDY I: FAULT DIAGNOSIS

The bearing data set from CWRU was sampled with different simulated bearing conditions under varied working loads. The bearing condition was stable during the data acquisition of each subset, thus a number of instantaneous bearing conditions were acquired, which is adequate to verify the robustness and discriminability of the developed perceptual vibration hashing method.

1) BEARING VIBRATION DATA

Specifically, four bearing conditions were simulated with 4 levels of working load, which included 3 faulty types (60 subsets in Table 2) and the normal type (4 subsets in Table 3). The 3 faulty types were inner race fault (IRF), ball fault (BF), and outer race fault (ORF). Four levels of fault severity were also simulated by introducing four crack diameters (0.007, 0.014, 0.021, and 0.028 in) to the inner races, balls of bearings by electro-discharge machining, while only the first three diameters were introduced to the outer races but with varied positions (@6:00, @3:00, and @12:00 o'clock). The working loads were measured by a torque sensor on the shaft. An accelerometer was installed on the motor housing at the drive end, and a 16-channel DAT recorder was used for data acquisition. A benchmark study was presented in [38], in which three manual diagnostic methods were performed and compared to make the discriminability of these vibration data more clear.

2) PERCEPTUAL VIBRATION HASHING

In this verification, 118 samples of non-overlapping vibration data were selected from each subset in Tables 2 and 3, and each sample had 1024 data points. Following the perceptual vibration hashing procedures listed in Section IV (Fig.4), all these samples were transformed into machine condition hashes.

In order to illustrate the procedures of perceptual vibration hashing in detail, 4 samples of vibration signals (see Fig. 5) were chosen as examples, which were the data sampled under the working load of 0 hp but with different bearing conditions: normal (Normal_0), inner race fault (IR007_0), ball fault (B007_0), and outer race fault (OR007_0).

TABLE 2. Faulty bearing dataset from Case Western Reserve University.

Fault Diameter(in)	Motor Load (hp)	Motor Speed (rpm)	Inner Race	Ball	Outer Race		
					@6:00	@3:00	@12:00
0.007"	0	1797	IR007_0	B007_0	OR007@6_0	OR007@3_0	OR007@12_0
	1	1772	IR007_1	B007_1	OR007@6_1	OR007@3_1	OR007@12_1
	2	1750	IR007_2	B007_2	OR007@6_2	OR007@3_2	OR007@12_2
	3	1730	IR007_3	B007_3	OR007@6_3	OR007@3_3	OR007@12_3
0.014"	0	1797	IR014_0	B014_0	OR014@6_0	*	*
	1	1772	IR014_1	B014_1	OR014@6_1	*	*
	2	1750	IR014_2	B014_2	OR014@6_2	*	*
	3	1730	IR014_3	B014_3	OR014@6_3	*	*
0.021"	0	1797	IR021_0	B021_0	OR021@6_0	OR021@3_0	OR07@12_0
	1	1772	IR021_1	B021_1	OR021@6_1	OR021@3_1	OR021@12_1
	2	1750	IR021_2	B021_2	OR021@6_2	OR021@3_2	OR021@12_2
	3	1730	IR021_3	B021_3	OR021@6_3	OR021@3_3	OR021@12_3
0.028"	0	1797	IR028_0	B028_0	*	*	*
	1	1772	IR028_1	B028_1	*	*	*
	2	1750	IR028_2	B028_2	*	*	*
	3	1730	IR028_3	B028_3	*	*	*

* There was no available dataset.

TABLE 3. Normal bearing dataset from Case Western Reserve University.

Fault Diameter(in)	Motor Load (hp)	Motor Speed (rpm)	Normal Data
0	0	1797	Normal_0
	1	1772	Normal_1
	2	1750	Normal_2
	3	1730	Normal_3

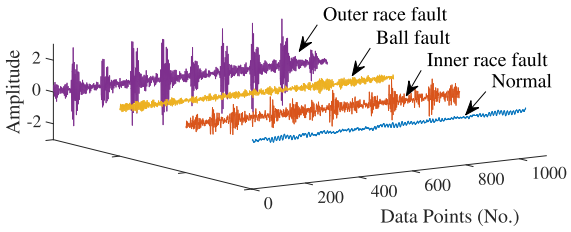

FIGURE 5. Vibration samples from 4 bearing conditions: normal (Normal_0), inner race fault (IR007_0), ball fault (B007_0) and outer race fault (OR007@6_0).

Firstly, each vibration sample in Fig. 5 was mapped into 32 sub-bands (or frequency bands) by WPT, i.e., WPT tree depth $j = 5$. From the viewpoint of filter banks, for a vibration signal acquired with a sampling frequency of 12 kHz, its Nyquist frequency will be 6 kHz, then the bandwidth of each sub-band is 187.5 Hz. In the leaf nodes, the sub-band signals were reconstructed and plotted into color maps in Fig. 6. Comparing these four colored maps of sub-band signals, it can be seen that there are different patterns of frequency concentration along the vertical axes, but there is no uniform distribution along the horizontal axes due to the time-frequency localization ability of WPT.

Secondly, in order to obtain a uniform pattern in the frequency distribution, each reconstructed sub-band signal was truncated into 4 blocks to apply the 2D-DCT. Then, the sum of absolute values of the 2D-DCT coefficients was extracted from each block as a sub-band feature, so a 128-dimensional sub-band feature vector can be built by cascading the features from the 32 sub-bands. Following the same feature extraction procedures, all the 118 data samples in each subset (Normal_0, IR007_0, B007_0, and OR007@6_0) were turned into sub-band features as shown in Fig. 7.

By 2D-DCT and feature extraction, a specific color map, such as the one shown in Fig. 6a, was condensed into a 128-dimensional sub-band feature in Fig. 7a. Recall that the sub-band features were extracted from the 2D-DCT coefficients in sub-bands, so a sub-band feature can still be interpreted as the frequency distribution from 0 to 6 kHz in the signal domain. Fig. 7 shows that the 118 sub-band features under the same bearing conditions exhibit a unique and consistent pattern. The predominant frequency components of normal bearings (Fig. 7a) distribute in the lower half, which makes it different from faulty bearings in Figs. 7b - 7d. Whereas for the faulty bearings, their frequency distribution patterns can also be easily distinguished: there is a clear concentration from 50 to 80 for the outer race fault, but some

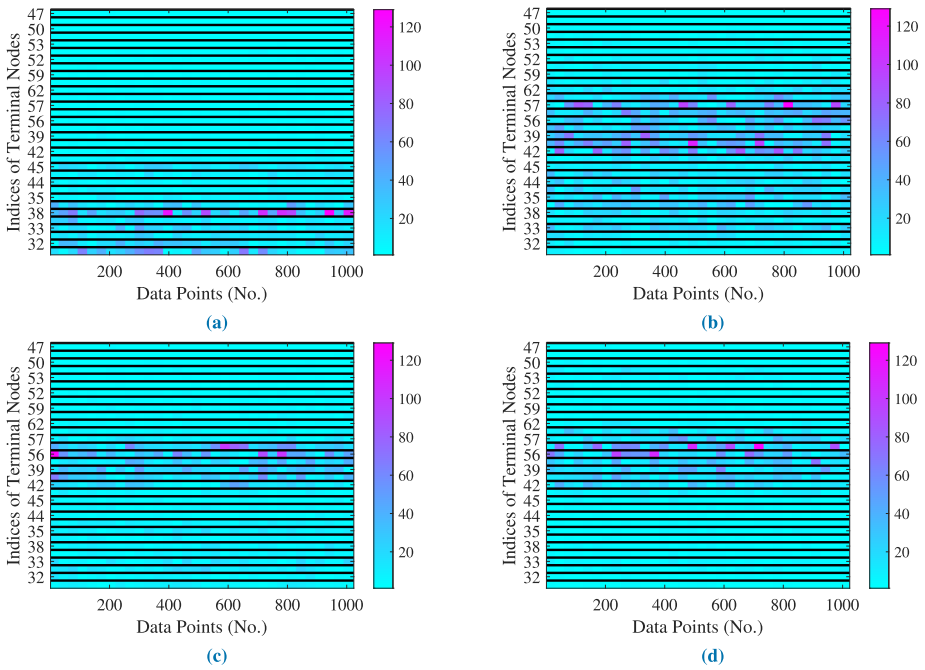

FIGURE 6. Reconstructed coefficients at the leaf nodes for 5-level wavelet packet transform (WPT), corresponding to the 4 bearing samples in Fig. 5. Each note represents a band of 187.5 Hz ($12000 \div 2 \div 2^5 = 187.5$) and the color represents the amplitude of coefficients. (a) Normal. (b) Inner race fault. (c) Ball fault. (d) Outer race fault.

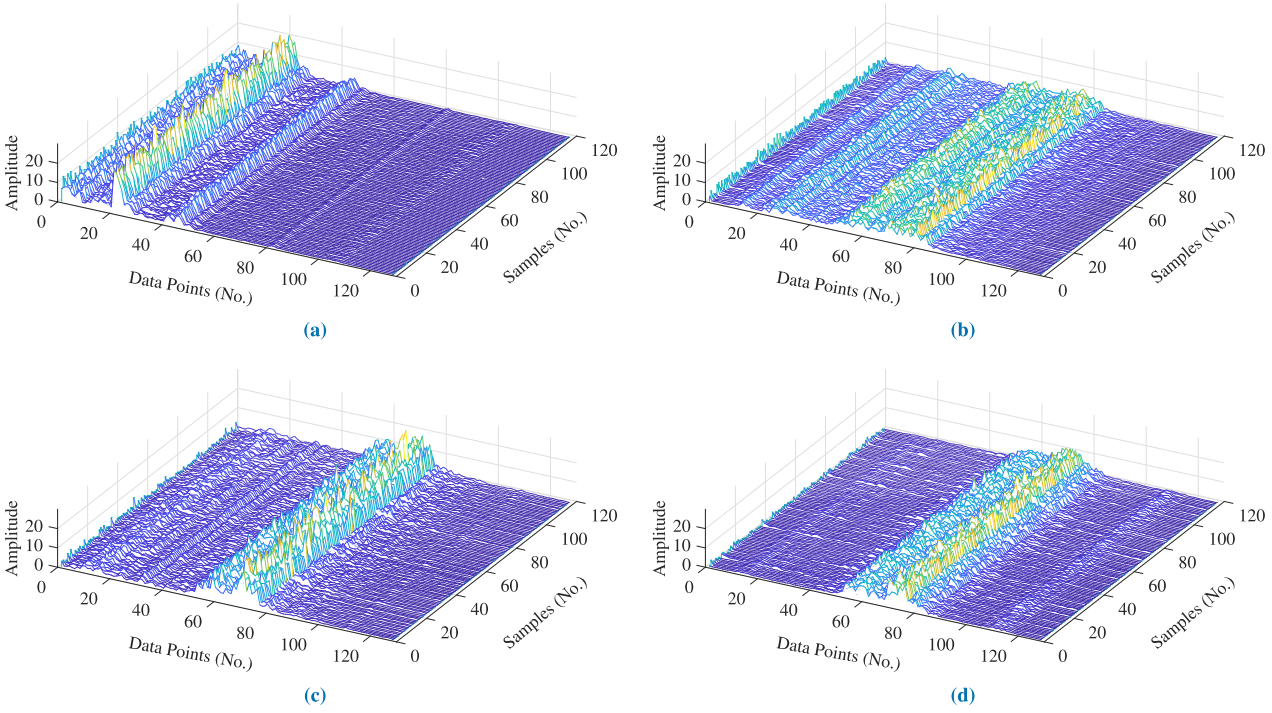

FIGURE 7. Waterfall plots of sub-band features for signals under 0 hp and 0.007 in of fault diameter. (a) Normal (Normal_0). (b) Inner race fault (IR007_0). (c) Ball fault (B007_0). (d) Outer race fault (OR007_0).

extra relatively low-frequency components appear in the ball fault, while the distribution of frequency components is more diffuse for the inner race fault.

Finally, the sub-band features can be hashed with SAX. Here, the sub-band features extracted from the 4 vibration samples in Fig. 5 are used for demonstration again, and their hashing procedures are illustrated in Fig. 8, in which 16 segments were used for the PAA and an alphabet size of 8 was used for symbolic representation. Taking the SAX hashing in Fig. 8a as an example, PAA was conducted among the 16 segments, and PAA coefficient in each segment was calculated with (3); then 7 breakpoints separated the value

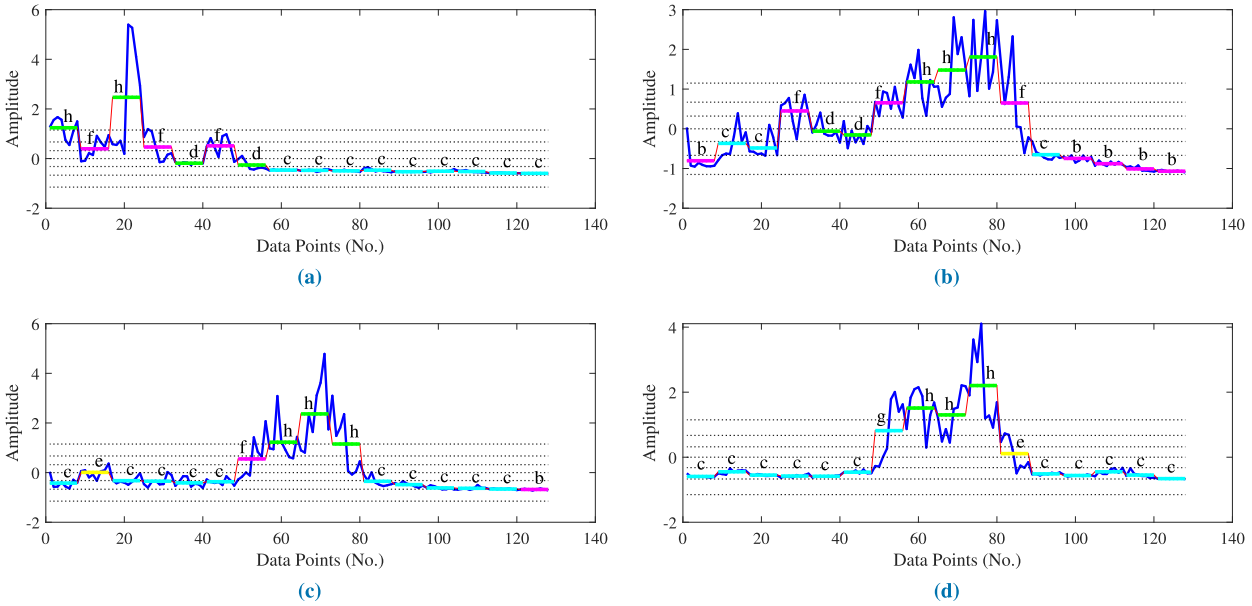

FIGURE 8. Illustration of SAX hashing for the 4 sub-band features extracted from the 4 vibration samples in Fig. 5. (a) Normal. (b) Inner race fault. (c) Ball fault. (d) Outer race fault.

TABLE 4. Diagnostic accuracy of the Case Western Reserve University faulty bearing dataset.

Fault Diameter(in)	Motor Load (hp)	Motor Speed (rpm)	Inner Race	Ball	Outer Race		
					@6:00	@3:00	@12:00
0.007"	0	1797	100.00	100.00	100.00	99.30	99.80
	1	1772	100.00	100.00	100.00	99.80	100.00
	2	1750	100.00	100.00	100.00	99.90	99.70
	3	1730	100.00	100.00	100.00	100.00	100.00
0.014"	0	1797	99.10	97.90	100.00	*	*
	1	1772	99.60	99.60	100.00	*	*
	2	1750	96.00	98.50	100.00	*	*
	3	1730	99.10	100.00	100.00	*	*
0.021"	0	1797	100.00	100.00	98.80	100.00	98.80
	1	1772	100.00	99.80	99.50	100.00	99.40
	2	1750	100.00	100.00	99.50	100.00	100.00
	3	1730	100.00	100.00	100.00	100.00	98.50
0.028"	0	1797	100.00	99.80	*	*	*
	1	1772	100.00	100.00	*	*	*
	2	1750	100.00	99.30	*	*	*
	3	1730	100.00	100.00	*	*	*

* There was no available dataset.

range into 8 parts based on a Gaussian assumption in the distribution of values; and a PAA coefficient falling in one part of the value range was represented with one character, i.e., each segment was represented by a character from ''a'' to ''h''. As a result, the vibration sample under the normal condition in Fig. 5 was transformed into the machine condition hash {hfhfdfdcccccccc}.

3) BEARING FAULT DIAGNOSIS

The distance space of machine condition hashes makes bearing fault diagnosis feasible. In order to make the verification more interpretable, The k-nearest neighbor (k-NN) algorithm [39] was adopted for bearing fault diagnosis.

In this evaluation, all the data in Tables 2 and 3 were transformed into machine condition hashes. In total, there

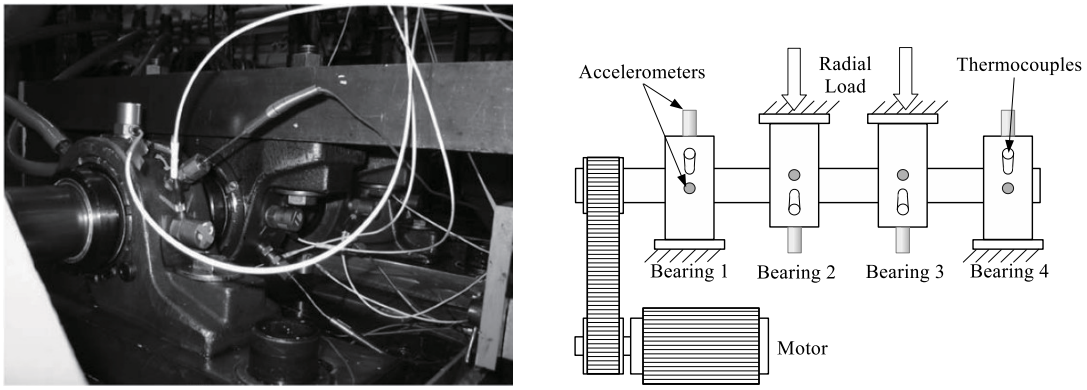

FIGURE 9. The bearing test stand used by the NSF Industry/University Cooperative Research Center for run-to-failure tests. (a) Picture. (b) Schematic diagram.

TABLE 5. Description of the bearing dataset from NSF Industry/University Cooperative Research Center.

Dateset (No.)	Test (No.)	Start	End	File Count	Recording Interval	Defected Bearing	Fault Type
D1	1	2003-10-22 12:06:24	2003-11-25 23:39:56	2156	10 min (5 min for first 43 files)	B3	IRF
D2						B4	BF
D3	2	2004-02-12 10:32:39	2004-02-19 06:22:39	984	10 min	B1	ORF
D4	3	2004-03-04 09:27:46	2004-04-04 19:01:57	4448	10 min	B3	ORF

were $118 \times (4 + 60) = 7552$ vibration samples evaluated. Half of the samples in each subset were randomly selected to train a k-NN classifier, while the others were left to be tested. The parameter k was set as $k = 9$, and the distance function in (5) was used for searching neighbors. Twenty rounds of classification tests were conducted, and the classification results for faulty conditions were averaged and listed in Table 4, while a classification accuracy of 100% was achieved for the normal bearing condition. Overall, the mean error rate of fault diagnosis is $0.7 \pm 0.24\%$.

Comparisons can be made instantly because many researchers have used the CWRU bearing dataset for method verification. Liang *et al.* [40] developed a systematic fault classification approach by a comprehensive feature fusion with deep belief network and sparse Bayesian extreme learning machine, which achieved a comparable classification accuracy of 99.3%. Zhang *et al.* [41] did a more extensive literature review on fault classification accuracy achieved with the CWRU bearing dataset, in which an overall classification accuracy above 92% is usually acceptable.

B. CASE STUDY II: DEGRADATION ASSESSMENT

The verification in Section V-A proves that perceptual vibration hashing is qualified for static fault classification, but condition monitoring is a substantially more complex dynamic process. In this section, the run-to-failure bearing vibration datasets from NSF Industry/University Cooperative Research Center (NSF I/UCRC) [37], which are also studied a lot in the PHM community, are used for degradation assessment.

1) RUN-TO-FAILURE BEARING VIBRATION DATA

The test rig (Fig. 9) used by the NSF I/UCRC can test 4 bearings simultaneously. A schematic diagram of the test rig is illustrated in Fig. 9b, while a closeup is shown in Fig. 9a, in which the installation of sensors is depicted in detail. The tested bearings were Rexnord ZA-2115 double-row bearings. The shaft supported by the 4 bearings was driven by an AC motor with a constant speed of 2000 rpm. A spring mechanism was designed and applied on the shaft to induce a radial load of 6000 lb. All bearings were force lubricated with an oil circulation system. In order to shut down the testing system automatically when a failure occurs, a magnetic plug was installed into the lubricating oil feedback pipe to collect metal debris. Then the electrical closing switch can be triggered when a certain level of debris is accumulated. The data acquisition scheme included a PCB 353B33 high-sensitivity quartz ICP accelerometer on each bearing housing, a National Instruments DAQCard-6062E data acquisition card, and the Labview software.

Three run-to-failure tests were conducted, and two faulty bearings were found in test 1, so 4 bearing datasets (D1 to D4 in Table 5) were acquired. The datasets D1 and D2 were acquired in test 1 with inner race fault (IRF) occurred on bearing B3 and ball fault (BF) occurred on bearing B4, respectively. Thus both D1 and D2 have 2156 files recorded.

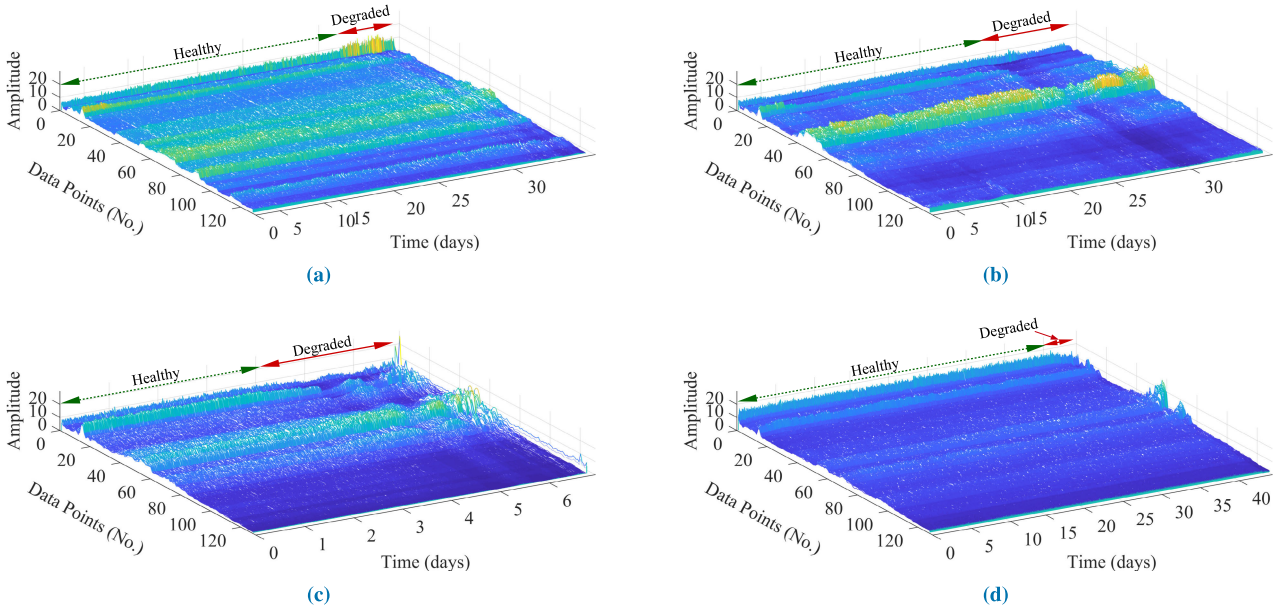

FIGURE 10. Feature evolution map of the 4 faulty bearings in Table 5, in which the extracted sub-band features were plotted against time in days to exhibit the dynamic evolution of bearing conditions. (a) Bearing B3 with IRF in test 1. (b) Bearing B4 with BF in test 1. (c) Bearing B1 with ORF in test 2. (d) Bearing B3 with ORF in test 3. NOTE: The tick labels of time axes in (a) and (b) are not equally spaced due to missing files.

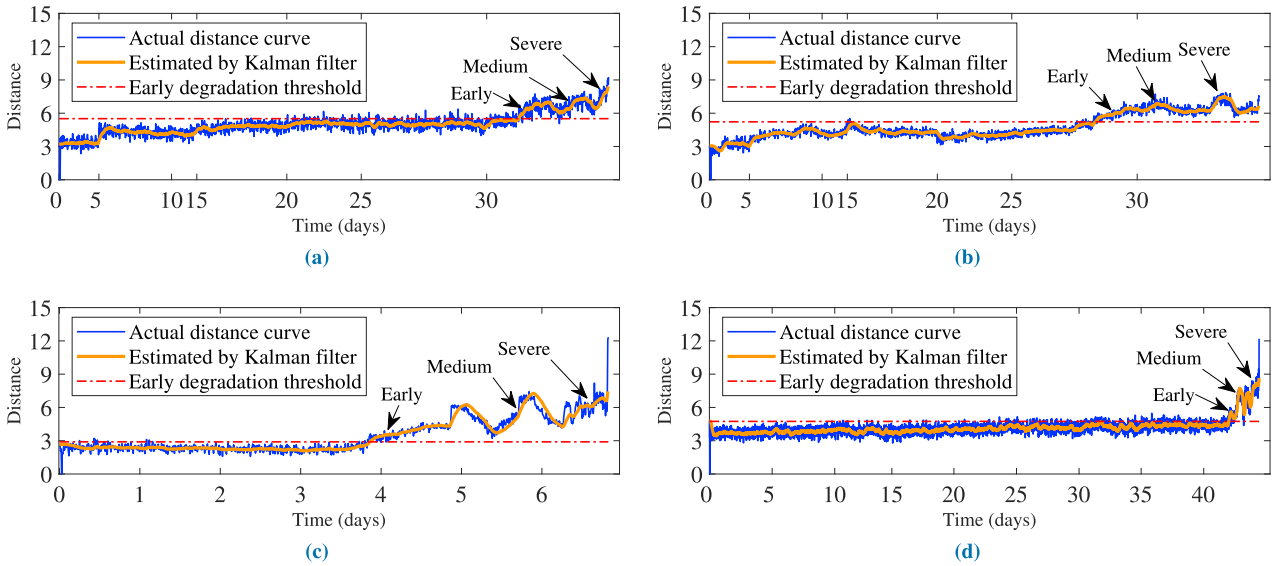

FIGURE 11. Distance curves of the 4 faulty bearings in Table 5 each with their first machine condition hash as the baseline, in which the actual distance curve is plotted in blue and the estimated curve by Kalman filter in orange. (a) Bearing B3 with IRF in test 1. (b) Bearing B4 with BF in test 1. (c) Bearing B1 with ORF in test 2. (d) Bearing B3 with ORF in test 3.

The dataset D3 has 984 vibration files, which were recorded in test 2 with outer race fault (ORF) found on bearing B1. There are 4448 vibration files in the dataset D4, also with ORF but on B3 from test 3. During each run-to-failure test, one-second vibration data were recorded every 10 min, except for the first 43 files in test 1 which had an interval of 5 min. The timestamp when each data file was recorded was used for vibration file naming. The sampling frequency was 20 kHz, so there were 20,480 data points for each channel of vibration data. A more detailed description of this experiment can be found in [42].

2) PERCEPTUAL VIBRATION HASHING

The run-to-failure bearing vibration data provide a good opportunity to investigate the dynamic evolution of the bearing condition. With the sub-band feature as a representation of the machine condition information, a feature evolution map

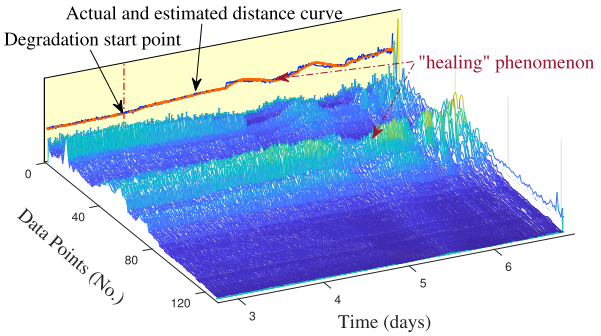

FIGURE 12. Conjoint analysis of the distance curve (Fig. 11c) and the feature evolution map (Fig. 10c) with degradation stage enlarged: the rise and fall of the distance curve reflects the deterioration and "healing" of the bearing condition.

can be obtained for each dataset by plotting the sub-band features with regard to time (Fig. 10).

During the feature extraction, 32 sub-bands were divided with 5-level WPT, and 4 blocks were truncated for 2D-DCT in each band, thus a 128-dimensional sub-band feature was extracted. Since each channel had 20,480 data points, it was truncated into 10 pieces for sub-band feature extraction, then an averaged sub-band feature was used in plotting the feature evolution map at a timestamp. In total, $2156 \times 2 + 984 + 4448 = 9744$ channels of vibration data were processed.

Fig. 10 shows that all the 4 feature evolution maps experience a stable stage before deformation. The fact is that the 4 faulty bearings all went through a period of normal running stage, but evolved into different faulty conditions. As explained in Section V-A.2, a sub-band feature can be interpreted as the frequency distribution pattern in a vibration signal. From this point of view, with the constant rotating speed and the fixed radial load, the frequency distribution should be stable during the normal running stage, but the stableness will be gradually undermined when an underlying degradation is in progress. Thus, the stable stages in the 4 feature evolution maps represent that the bearings are in healthy condition, and the deformations at the end of feature evolution maps are a reflection of degradation. With a further reference to other researchers' studies with the NSF I/UCRC data [42], [44], [45], it can be concluded that the dynamic change of the sub-band feature conforms to the evolution of bearing condition.

The "healing" phenomenon also exemplifies the effectiveness of sub-band feature in revealing the machine condition information. As explained in [42] and [43], the sharp edges of a crack or small damage zone could be further smoothed by the continuous rolling contact during the degradation process. So the feature evolution map deforms because of the emerging cracks, but then restores somewhat due to the "healing" phenomenon. This is substantially reflected both in Figs. 10b and 10c. Moreover, the smoothness in the deformation and restoration indicates that the developed feature extraction method has a good resolution (discriminability) in detecting weak changes in the bearing conditions.

All the sub-band features in Fig. 10 were further transformed into machine condition hashes by SAX with a 32-segment PAA and an alphabet size of 8 for symbolic representation.

3) DEGRADATION ASSESSMENT WITH DISTANCE CURVE

If the sub-band feature can reveal the machine condition information steadily and precisely, the generated machine condition hash will naturally be a more compact representation of the machine condition information. The distance metric against the healthy machine condition hash would then provide a quantitative assessment of the degradation.

By setting the first machine condition hash of each bearing as the baseline of a healthy bearing, the distance metrics of the subsequent machine condition hashes were calculated for the 4 bearings with (5). Then the results (blue curve) were also plotted with regard to time in Fig. 11.

Comparing Fig. 11 with 10, it can be concluded that the increasing trend in the distance metric indicates the degradation of a bearing. Firstly, the distance values in a curve remain at a relatively stable low value before increasing, which indicates that the bearing maintains a healthy status before degradation. Secondly, the fluctuations at the end of the distance curves correspond to the shape deformations of the feature evolution maps in Fig. 10. An example is shown in Fig. 12, in which the distance curve in Fig. 11c is plotted together with the feature evolution map in Fig. 10c by enlarging the degradation stage. It is clear that, from the degradation start point, the deformation in the feature evolution map causes the fluctuation in the distance curve. Lastly, when the feature evolution map almost restores its original shape, the distance values go down, which is indeed a reflection of the "healing" phenomenon.

4) CONSIDERATIONS ON CONDITION MONITORING APPLICATION

The above demonstrations show that the distance curve can be an effective tool for real-time monitoring of machine condition. The following considerations may further help in improving and understanding the distance curve in condition monitoring applications:

Firstly, Due to the complexity of rotational dynamics and kinematics, and also taking environmental interference into consideration, noises in the actual distance curve are unavoidable. Also considering that the degradation of the bearing condition is virtually an accumulative process, a reasonable solution for noise cancellation is to apply the Kalman filter to estimate the current distance value based on past observations. The estimated curves plotted in orange in Fig. 11 exhibit a stable indication of bearing conditions.

Secondly, a threshold can be issued based on empirical observations so that the early degradation can be detected automatically. Intuitively, this threshold can be determined based on distance values at a relatively stable stage.

For example, the thresholds in Fig. 11 were set as 1.3 times the mean distance values at the bearings' stable middle stages.

Thirdly, the distance metric generally increases when a bearing degrades, but this degradation does not always increase with time. Bearing degradation turns out to be a complex process, such as the ''healing'' phenomenon prolonging the degradation process in Fig. 11c.

Finally, the bearing condition will inevitably degrade, so the distance curve still rises. As it is denoted (with reference to [45]) in Fig. 10, when the degradation progresses from ''early ''to ''medium'' and then ''severe'', the distance value of the machine condition hashes can also indicate the level of degradation.

VI. DISCUSSION AND CONCLUSION

In order to overcome the problem of low efficiency caused by high data throughput in real-time vibration monitoring, this paper developed a sub-band coding method for perceptual hashing vibration signals so that compact machine condition hashes are transmitted instead of the raw vibration signals. Fault diagnosis and prognosis can both be achieved by inferring in the distance space of machine condition hashes.

Sub-band coding is a general signal processing scheme followed in this paper to extract and represent the machine condition information. Following the same scheme, other signal processing techniques that are capable of dividing frequency bands and extracting feature can also be investigated, such as sparse coding and empirical mode decomposition. The wavelet packet transform and two-dimensional discrete cosine transform are adopted in this paper mostly because their computation efficiency, of which the computational complexities of their fast algorithms are summarized in Section III. However, when deploying them in edge computing applications, measures that can further improve computing efficiency deserve a further study. For example, the lifting-based wavelet packet transform [46] can be adopted for faster and in-place calculation [47], or implemented with digital signal processors or filter bank circuits.

The effectiveness of the developed perceptual vibration hashing method was verified with two benchmark bearing datasets. The CWRU bearing dataset was used for bearing fault diagnosis, in which an overall diagnostic accuracy of 99.3% was achieved using a k-NN classifier, while the degradation assessment on the NSF I/UCR Center showed that the dynamic degradation process of bearings could be tracked with the distance curve of machine condition hashes. In fact, more sophisticated fault diagnostic/prognostic method [48] can be investigated in the distance space constructed by machine condition hashes. For instance, a robust regression curve fitting approach can be applied to predict the reminding useful life of components [49].

The efficiency of condition monitoring can benefit from the compactness of the machine condition hash. Transforming a 1024-point (4-byte float type) vibration signal into a 32-byte machine condition hash, the ratio of data dimension reduction is 1/128, thus the network bandwith, data storage space, and communication costs can be saved. Furthermore, deploying the perceptual vibration hashing method on a terminal, the computation burden is also relieved from the central server to the monitoring terminal.

Different distance functions can be defined for machine condition inference on the server. In this way, a diagnostic model is decoupled into the machine condition hash generation on the terminal and the condition inference on the server. Thus, flexibility in diagnostic and prognostic modeling is also achieved.

In conclusion, by perceptual vibration hashing, the extracted sub-band features can effectively reveal the frequency distribution pattern in the vibration signals, which are further compacted and symbolically represented by the machine condition hash. With the compact machine condition hashes generated, transmitted, stored, and inferred on, the demands for efficiency and effectiveness in condition monitoring are balanced.

REFERENCES

[1] L. Wang and X. V. Wang, ''Condition monitoring for predictive maintenance,'' in *Cloud-Based Cyber-Physical Systems in Manufacturing*, L. Wang and X. V. Wang, Eds. Cham, Switzerland: Springer, 2018, pp. 163–192.
[2] Z. Zhou, B. Yao, W. Xu, and L. Wang, ''Condition monitoring towards energy-efficient manufacturing: A review,'' *Int. J. Adv. Manuf. Technol.*, vol. 91, nos. 9–12, pp. 3395–3415, 2017.
[3] S. Yang, B. Bagheri, H.-A. Kao, and J. Lee, ''A unified framework and platform for designing of cloud-based machine health monitoring and manufacturing systems,'' *J. Manuf. Sci. Eng.*, vol. 137, no. 4, 2015, Art. no. 040914.
[4] W. Shi, J. Cao, Q. Zhang, Y. Li, and L. Xu, ''Edge computing: Vision and challenges,'' *IEEE Internet Things J.*, vol. 3, no. 5, pp. 637–646, Oct. 2016.
[5] M. D. de Assunção, A. da Silva Veith, and R. Buyya, ''Distributed data stream processing and edge computing: A survey on resource elasticity and future directions,'' *J. Netw. Comput. Appl.*, vol. 103, pp. 1–17, Feb. 2017.
[6] R. Yan, R. X. Gao, and X. Chen, ''Wavelets for fault diagnosis of rotary machines: A review with applications,'' *Signal Process.*, vol. 96, pp. 1–15, Mar. 2014.
[7] J. Chen, Z. Li, J. Pan, G. Chen, Y. Zi, J. Yuan, B. Chen, and Z. He, ''Wavelet transform based on inner product in fault diagnosis of rotating machinery: A review,'' *Mech. Syst. Signal Process.*, vols. 70–71, pp. 1–35, Mar. 2016.
[8] Y. Lei, J. Lin, Z. He, and M. J. Zuo, ''A review on empirical mode decomposition in fault diagnosis of rotating machinery,'' *Mech. Syst. Signal Process.*, vol. 35, nos. 1–2, pp. 108–126, Feb. 2013.
[9] J. Antoni and R. Randall, ''The spectral kurtosis: Application to the vibratory surveillance and diagnostics of rotating machines,'' *Mech. Syst. Signal Process.*, vol. 20, no. 2, pp. 308–331, 2006.
[10] P. Boškoski, M. Gašperin, D. Petelin, and D. Juričić, ''Bearing fault prognostics using Rényi entropy based features and Gaussian process models,'' *Mech. Syst. Signal Process.*, vols. 52–53, no. 1, pp. 327–337, 2015.
[11] A. Malhi and R. X. Gao, ''PCA-based feature selection scheme for machine defect classification,'' *IEEE Trans. Instrum. Meas.*, vol. 53, no. 6, pp. 1517–1525, Dec. 2004.
[12] T. W. Rauber, F. de A. Boldt, and F. M. Varejão, ''Heterogeneous feature models and feature selection applied to bearing fault diagnosis,'' *IEEE Trans. Ind. Electron.*, vol. 62, no. 1, pp. 637–646, Jan. 2015.
[13] K. Worden, W. J. Staszewski, and J. J. Hensman, ''Natural computing for mechanical systems research: A tutorial overview,'' *Mech. Syst. Signal Process.*, vol. 25, no. 1, pp. 4–111, 2011.
[14] Y. Cao, H. Qi, W. Zhou, J. Kato, K. Li, X. Liu, and J. Gui, ''Binary hashing for approximate nearest neighbor search on big data: A survey,'' *IEEE Access*, vol. 6, pp. 2039–2054, 2017.
[15] J. Wang, T. Zhang, J. Song, N. Sebe, and H. T. Shen, ''A survey on learning to hash,'' *IEEE Trans. Pattern Anal. Mach. Intell.*, vol. 40, no. 4, pp. 769–790, Apr. 2018.

[16] X.-M. Niu and Y.-H. Jiao, "An overview of perceptual hashing," *Acta Electron. Sinica*, vol. 36, no. 7, pp. 1405–1411, 2008.
[17] H. Liu, X. Men, F. Li, J. Zhang, X. Wang, and C. Liu, "A new methodology for condition monitoring based on perceptual hashing," in *Proc. IEEE 13th ICIEA*, Wuhan, China, 2018, pp. 919–923.
[18] R. E. Crochiere, S. A. Webber, and J. L. Flanagan, "Digital coding of speech in sub-bands," *Bell Syst. Tech. J.*, vol. 55, no. 8, pp. 1069–1085, Oct. 1976.
[19] A. Croisier, D. Esteban, and C. Galand, "Perfect channel splitting by use of interpolation/decimation/tree decomposition techniques," in *Proc. Int. Symp. Inf. Circuis Syst.*, 1976, pp. 443–446.
[20] M. Vetterli and J. Kovačević, *Wavelets and Subband Coding*. Englewood Cliffs, NJ, USA: Prentice-Hall, 1995.
[21] G. Stoll and Y.-F. Dehery, "High quality audio bit-rate reduction system family for different applications," in *Proc. IEEE Int. Conf. Commun., Including Supercomm Tech. Sessions*, Apr. 2002, pp. 937–941.
[22] Y. F. Dehery, M. Lever, and P. Urcun, "A MUSICAM source codec for digital audio broadcasting and storage," in *Proc. Int. Conf. Acoust., Speech, Signal Process.*, vol. 5, Apr. 1991, pp. 3605–3608.
[23] M. Vetterli and C. Herley, "Wavelets and filter banks: Theory and design," *IEEE Trans. Signal Process.*, vol. 40, no. 9, pp. 2207–2232, Sep. 1992.
[24] M. Stéphane, *A Wavelet Tour of Signal Processing: The Sparse Way*, 3rd ed. Burlington, MA, USA: Elsevier, 2009.
[25] M. Hamidi and J. Pearl, "Comparison of the cosine and Fourier transforms of Markov-1 signals," *IEEE Trans. Acoust., Speech, Signal Process.*, vol. 24, no. 5, pp. 428–429, Oct. 1976.
[26] N. Ahmed, T. Natarajan, and K. R. Rao, "Discrete cosine transform," *IEEE Trans. Comput.*, vol. C-23, no. 1, pp. 90–93, Jan. 1974.
[27] X. Shao and S. G. Johnson, "Type-II/III DCT/DST algorithms with reduced number of arithmetic operations," *Signal Process.*, vol. 88, no. 6, pp. 1553–1564, 2008.
[28] J. Lin, E. Keogh, S. Lonardi, and B. Chiu, "A symbolic representation of time series, with implications for streaming algorithms," in *Proc. 8th ACM SIGMOD Workshop Res. Issues Data Mining Knowl. Discovery (DMKD)*, San Diego, CA, USA, 2003, pp. 2–11.
[29] E. Keogh, K. Chakrabarti, M. Pazzani, and S. Mehrotra, "Dimensionality reduction for fast similarity search in large time series databases," *Knowl. Inf. Syst.*, vol. 3, no. 3, pp. 263–286, Aug. 2001.
[30] S. Lonardi, "Global detectors of unusual words: Design, implementation, and applications to pattern discovery in biosequences," Ph.D. dissertation, Dept. Comput. Sci., Purdue Univ., West Lafayette, IN, USA, Aug. 2001.
[31] A. Apostolico, M. E. Bock, and S. Lonardi, "Monotony of surprise and large-scale quest for unusual words," *J. Comput. Biol.*, vol. 10, nos. 3–4, pp. 283–311, Jun. 2003.
[32] C. Faloutsos, M. Ranganathan, and Y. Manolopoulos, "Fast subsequence matching in time-series databases," *ACM SIGMOD Rec.*, vol. 23, no. 2, pp. 419–429, Jun. 1994.
[33] E. C. Smith and M. S. Lewicki, "Efficient auditory coding," *Nature*, vol. 439, no. 7079, pp. 978–982, 2006.
[34] B. A. Olshausen and C. J. Rozell, "Neuromorphic computation: Sparse codes from memristor grids," *Nature Nanotechnol.*, vol. 12, no. 8, pp. 722–723, Aug. 2017.
[35] K. Okada, F. Rong, J. Venezia, W. Matchin, I.-H. Hsieh, K. Saberi, J. T. Serences, and G. Hickok, "Hierarchical organization of human auditory cortex: Evidence from acoustic invariance in the response to intelligible speech," *Cerebral Cortex*, vol. 20, no. 10, pp. 2486–2495, 2010.
[36] K. Loparo. *Case Western Reserve University Bearing Data Center*. Accessed: Apr. 10, 2019. [Online]. Available: https://csegroups.case.edu/bearingdatacenter/pages/welcome-case-western-reserve-university-bearing-data-center-website
[37] J. Lee, H. Qiu, G. Yu, and J. Lin. (2007). *Rexnord Technical Services, Bearing Data Set IMS, NASA Ames Prognostics Data Repository. University of Cincinnati*. Accessed: Apr. 10, 2019. [Online]. Available: http://ti.arc.nasa.gov/tech/dash/pcoe/prognostic-data-repository/
[38] W. A. Smith and R. B. Randall, "Rolling element bearing diagnostics using the Case Western Reserve University data: A benchmark study," *Mech. Syst. Signal Process.*, vols. 64–65, pp. 100–131, Dec. 2015.
[39] N. S. Altman, "An introduction to kernel and nearest-neighbor nonparametric regression," *Amer. Statist.*, vol. 46, no. 3, pp. 175–185, Aug. 1992.
[40] J. Liang, Y. Zhang, J.-H. Zhong, and H. Yang, "A novel multi-segment feature fusion based fault classification approach for rotating machinery," *Mech. Syst. Signal Process.*, vol. 122, pp. 19–41, May 2019.
[41] X. Zhang, Y. Liang, and J. Zhou, "A novel bearing fault diagnosis model integrated permutation entropy, ensemble empirical mode decomposition and optimized SVM," *Measurement*, vol. 69, pp. 164–179, Jun. 2015.
[42] H. Qiu, J. Lee, J. Lin, and G. Yu, "Robust performance degradation assessment methods for enhanced rolling element bearing prognostics," *Adv. Eng. Inform.*, vol. 17, nos. 3–4, pp. 127–140, Jul./Oct. 2003.
[43] T. Williams, X. Ribadeneira, S. Billington, and T. Kurfess, "Rolling element bearing diagnostics in run-to-failure lifetime testing," *Mech. Syst. Signal Process.*, vol. 15, no. 5, pp. 979–993, 2001.
[44] J. Yu, "Health condition monitoring of machines based on hidden Markov model and contribution analysis," *IEEE Trans. Instrum. Meas.*, vol. 61, no. 8, pp. 2200–2211, Aug. 2012.
[45] S. Wang, G. Cai, Z. Zhu, W. Huang, and X. Zhang, "Transient signal analysis based on Levenberg–Marquardt method for fault feature extraction of rotating machines," *Mech. Syst. Signal Process.*, vol. 54, pp. 16–40, Mar. 2015.
[46] W. Sweldens, "The lifting scheme: A construction of second generation wavelets," *SIAM J. Math. Anal.*, vol. 29, no. 2, pp. 511–546, Mar. 1998.
[47] Y. Huang, C. Liu, X. F. Zha, and Y. Li, "An enhanced feature extraction model using lifting-based wavelet packet transform scheme and sampling-importance-resampling analysis," *Mech. Syst. Signal Process.*, vol. 23, no. 8, pp. 2470–2487, 2009.
[48] J. Lee, F. Wu, W. Zhao, M. Ghaffari, L. Liao, and D. Siegel, "Prognostics and health management design for rotary machinery systems—Reviews, methodology and applications," *Mech. Syst. Signal Process.*, vol. 42, nos. 1–2, pp. 314–334, 2014.
[49] D. Siegel, C. Ly, and J. Lee, "Methodology and framework for predicting helicopter rolling element bearing failure," *IEEE Trans. Rel.*, vol. 61, no. 4, pp. 846–857, Dec. 2012.

HAINING LIU received the B.S. degree in mechanical engineering from Shandong University, Jinan, China, in 2005, and the Ph.D. degree in mechatronic engineering from Shanghai Jiao Tong University, Shanghai, China, in 2011. Since 2019, he has been a Visiting Scholar with the Center for Advanced Life Cycle Engineering (CALCE), University of Maryland at College Park, MD, USA. He is currently with the School of Mechanical Engineering, University of Jinan. His research interests include prognostics and health management, vibration signal processing, big data analysis, and condition monitoring technologies for industrial applications.

YIXIANG WANG is currently pursuing the degree with the School of Mechanical Engineering, University of Jinan, Jinan, China. He has been involved in several research projects since his sophomore year, and participated in the vibration data analysis work in this article.

FAJIA LI received the B.S. degree in mechanical engineering and the M.S. degree in agricultural mechanization engineering from the Shandong University of Technology, Zibo, China, in 2005 and 2009, respectively, and the Ph.D. degree in mechanical design and theory from the Nanjing University of Aeronautics and Astronautics, Nanjing, China, in 2015. He is currently with the School of Mechanical Engineering, University of Jinan. His research interests include mechanical dynamics, vibration testing, and fault diagnostics.

XIAOHONG WANG received the B.S. degree in automation from the Shandong Building Material College, Jinan, China, in 1983, the M.S. degree in control theory and application from the University of Chongqing, Chongqing, China, in 1987, and the Ph.D. degree in control theory and control engineering from Northeastern University, Shenyang, China, in 2014. He is currently a Professor with the School of Electrical Engineering, University of Jinan, and also a Taishan Scholar of the People's Government of Shandong Province. His research interests include industrial automation and intelligent manufacturing.

CHENGLIANG LIU received the Ph.D. degree in mechanical engineering from Southeast University, China, in 1999. Then, he joined as an Assistant Professor with the School of Mechanical Engineering, Institute of Robotics, Shanghai Jiao Tong University. In 2000, he was invited to the University of Cincinnati and the University of Wisconsin as a Senior Visiting Scholar. He was promoted to Professor, in 2002, taking charge of the Institute of Mechatronics. His research interests include intelligent robot systems, power electronics, MEMS application to precise agriculture, network-based monitoring, and GPS/GIS/RS-equipped apparatus/machinery. He was a twice recipient of the Award for the National Prize of Science and Technology Progress Grade II, China, in 2009 and 2011, respectively.

MICHAEL G. PECHT (S'78–M'83–SM'90–F'92) received the B.S. degree in physics, the M.S. degree in electrical engineering, and the M.S. and Ph.D. degrees in engineering mechanics from the University of Wisconsin–Madison, Madison, WI, USA, in 1976, 1978, 1979, and 1982, respectively.

He is currently the Founder and the Director of the Center for Advanced Life Cycle Engineering, University of Maryland at College Park, College Park, MD, USA, which is funded by more than 150 of the world's leading electronics companies at more than US6M/year. He is also a Chair Professor of mechanical engineering and a Professor of applied mathematics, statistics, and scientific computation with the University of Maryland at College Park. He has authored or coauthored more than 20 books, 400 technical articles, and holds eight patents.

He is Fellow of the American Society of Mechanical Engineers, of the Society of Automotive Engineers, and of the International Microelectronics Assembly and Packaging Society. He was the Editor-In-Chief of IEEE Access and served as the Chief Editor for the IEEE Transactions on Reliability for 9 years, and the Chief Editor for *Microelectronics Reliability* for 16 years. He has served on the three U.S. National Academy of Science studies, the two U.S. Congressional Investigations in Automotive Safety, and as an Expert for the U.S. Food and Drug Administration. He is a Professional Engineer of the American Society of Mechanical Engineers, the Society of Automotive Engineers, and the International Microelectronics Assembly and Packaging Society.